



Investigation of Adhesive Perception Based on Friction and Brain Activation

Xingxing Fang¹ · Wei Tang¹ · Shousheng Zhang¹ · Tengfei Zhuang¹

Received: 18 December 2023 / Revised: 8 April 2024 / Accepted: 10 April 2024 / Published online: 20 May 2024
© Jilin University 2024

Abstract

The enhancement of adhesive perception is crucial to maintaining a stable and comfortable grip of the skin-touch products. To study the tactile perception of adhesive surfaces, subjective evaluation, skin friction and vibrations, and neurophysiological response of the brain activity were investigated systematically. Silicone materials, which are commonly used for bionic materials and skin-touch products, were chosen for the tactile stimulus. The results showed that with the increasing of surface adhesion, the dominant friction transferred from a combination of adhesive friction and deformation friction to adhesive friction. The friction coefficient and vibration amplitude had strong correlations with the perceived adhesion of surfaces. The parietal lobe and occipital lobe were involved in adhesive perceptions, and the area and intensity of brain activation increased with the increasing surface adhesion. Surfaces with larger adhesion tended to excite a high P300 amplitude and short latency, indicating that the judgment was faster and that more attentional resources were involved in adhesive perception. Furthermore, the electroencephalograph signals of the adhesive perception were simulated by the neural mass model. It demonstrated that the excitability and intensity of brain activity, and the connectivity strength between two neural masses increased with the increasing surface adhesion. This study is meaningful to understand the role of surface adhesion in tactile friction and the cognitive mechanism in adhesive perception to improve the tactile experience of adhesive materials.

Keywords Surface adhesion · Tactile perception · Friction · Brain activation · Neural mass model

1 Introduction

Since the theory of adhesive friction was pioneered by Bowden and Tabor, there have been a growing number of studies confirming that interfacial adhesion is an important factor in sliding friction [1–4]. It is well known that adhesion and friction are correlated, and friction in the presence of adhesion is a critical issue in tribology [5, 6]. Currently, significant progress has been made in the adhesive characteristics and bionic surfaces based on the inspiration from organisms in nature [7–9], physics-based theories of adhesion are still very active in the study of soft materials and biomechanics [10–12]. The surface adhesion exhibits significant potential in many fields requiring flexible grasping and manipulation [13–16]. In tactile friction, the adhesion component has been demonstrated to contribute significantly

to the frictional force [17, 18]. A comprehensive understanding of the role of adhesion in tactile friction is crucial to maintaining a secure grip during manipulation of hand-held objects, where a large and stable friction force is needed to avoid undesired movement.

Silicone is a highly reactive adhesive material, and due to its soft texture, stable chemical properties, and great adhesion, silicone materials are widely used as bionic materials and in the manufacture of skin-touch products such as prosthetic socket, handles of labor and sporting goods, anti-slip pads, tablecloths, and phone cases to maintain a secure grip [19]. However, the functional features of the products gradually become saturated due to the fierce competition in the market, and the enhancement of tactile experience has become a new requirement. As an important carrier of information transfer, suitable tactile design can greatly enhance the market competitiveness of products [20].

Tactile perception arises from the frictional vibrations of the skin against a surface during the touch process and is ultimately formed in the somatosensory cortex of the cerebral cortex [21]. Researchers have revealed that the physical

✉ Wei Tang
tangwei@cumt.edu.cn

¹ School of Mechatronic Engineering, China University of Mining and Technology, Xuzhou 221116, Jiangsu, China

properties of materials and frictional vibrations significantly affect tactile perceptions [22], the friction coefficient, vertical deviation, and spectral centroid characteristic parameters were consistent with human tactile sensing, and the frictional vibration signals can be used to characterize the sensation of roughness and softness formed by the touching process [23, 24]. For the tactile perception of adhesion, Mith et al. suggested that a qualitative approach by a touch test can be used to study the adhesive perception, and the perceptual intensity judgements were correlated to the adhesion parameters [25, 26]. Furthermore, the cognitive mechanisms of the brain associated with the adhesive perception revealed that the activated brain area varied with the intensity of adhesion [27]. Recently, due to the advantages of high temporal resolution and low cost, Electroencephalograph (EEG) technologies have been widely used to assess neurophysiological response of the brain associated with the tactile perception [28–30]. It has been demonstrated that frictional vibration involved in tactile perception may cause neuronal entrainment in the brain, such as earlier somatosensory evoked potential components, and the P300 component of Event-related Potential (ERP) signals [31, 32]. However, EEG technology cannot be used to obtain the deep connection between brain activity and tactile perception, therefore, the Neural Mass Model (NMM) has been established by researchers to simulate the process of brain activity [33, 34]. By treating neurons with similar properties as a group and modeling them in terms of overall properties, NMM can be used to further explain the cognitive mechanism of tactile perception reveal the specific information transmission mechanism and brain activity between the neural masses during the tactile perception of adhesion.

Friction in the presence of adhesion is a critical problem in tribology, and while the perception of adhesion is one of the fundamental dimensions for tactile perception, little has been clarified about adhesive perception and its neural mechanisms. This investigation systematically studied adhesive perception based on subjective evaluation, friction and

vibration, and brain activity. Silicone samples with different adhesion features were prepared. The surface adhesion that influenced the friction coefficients, vibration amplitudes, and adhesive tactile perceptions were analyzed, and the related friction mechanism was discussed. To determine the brain area and the neural activity involved in adhesive perception, ERP signals of the brain activated by different adhesive surface were measured. Furthermore, a NMM was established to simulate the feedback of brain neurons to adhesive perceptions, and the mechanism of the formation of adhesive perception was revealed.

2 Experimental Details

2.1 Samples

The adhesion features of the samples were determined by the degree of liquid silica gel. The higher the degree of liquid silica gel, the lower the adhesion of the prepared samples. First, 0-degree and 80-degree liquid silica gels were mixed at different ratios to form 10, 30, 50, and 70-degree formulated liquid silica gels, respectively. Then, the curing agent and silicone oil were added to the formulated liquid silica gel to form the tactile samples with the size of 50 mm × 30 mm × 3 mm by the turnover formwork. Figure 1 shows the microscopy images of samples, and Table 1 shows the preparation ratios and physical properties of the silicone samples. The hardness of the samples was measured by a shore hardness tester A (Bareiss, Germany). The pressure probe was quickly pressed vertically onto the sample surface, and five measurements were taken at different locations on the surface to obtain an average. An electro-mechanical universal testing machine (MTS, Shanghai, China) was used to measure the elastic parameters of the samples. A tensile force was applied to the sample and the strain was measured, Young's modulus was obtained by calculating the ratio of the stresses and strains, and Poisson's ratio was calculated

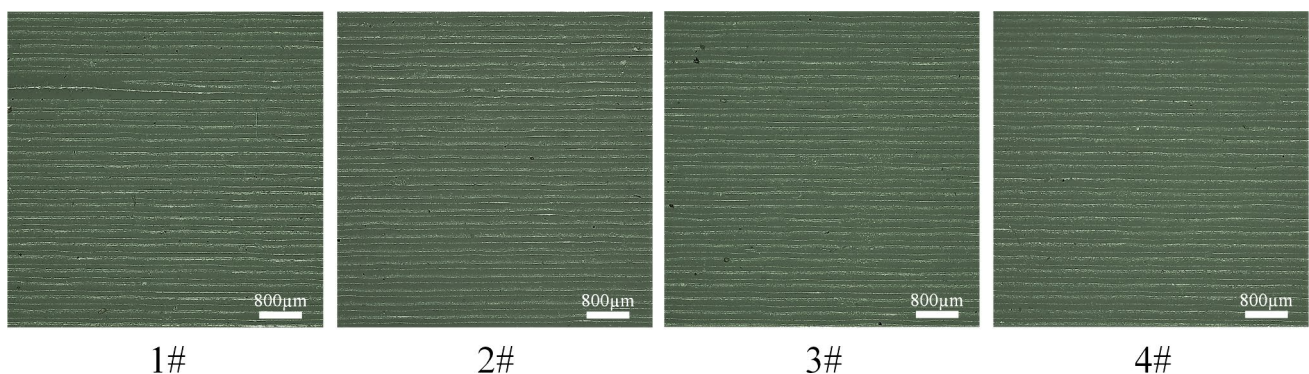


Fig. 1 Surface microscopy images of silicone samples

Table 1 Physical properties of samples

Samples	1#	2#	3#	4#
80-degree silica gel: 0-degree silica gel	1:7	1:1.67	1:0.6	1:0.14
Curing agent /%	3	2	1.5	1
Silicone oil /%	0	1	2	3
Hardness /HS	9.7±0.2	28.4±0.3	50.9±0.4	70.9±0.1
Young's modulus /MPa	0.47	0.86	1.57	2.87
Poisson's ratio	0.43	0.46	0.48	0.48
Surface roughness $Ra/\mu\text{m}$	0.83±0.03	0.82±0.04	0.80±0.04	0.78±0.03

from the longitudinal and transverse strains. The surface roughness of the samples was measured by an OLS5100-3D laser microscope (Olympus, Tokyo, Japan).

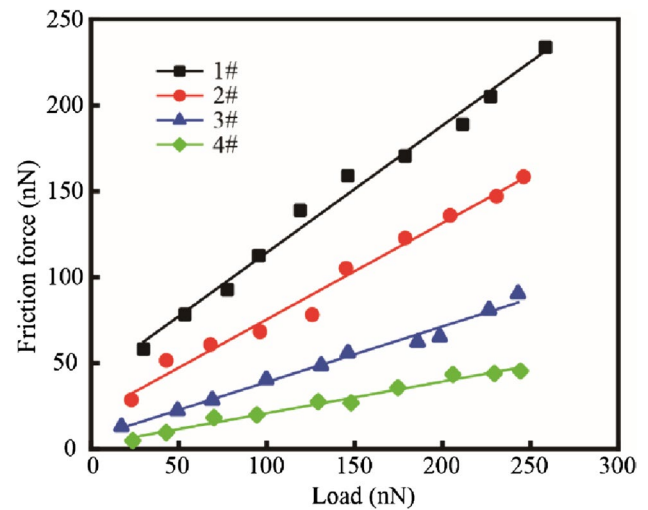
Atomic Force Microscopy (AFM) is a powerful device to investigate the surface mechanical properties and for the characterization of surface forces, and AFM has also been directly used in adhesion studies by analysis of the continuous tip–surface interaction during the measurement [35, 36]. The adhesion of the surfaces can be characterized by calculating the horizontal intercept of the friction force versus normal load curve, since the friction force F is guided by the following equation [37]:

$$F = \mu(W + F_a) \quad (1)$$

where μ is the friction coefficient, W is the normal load, and F_a is the adhesive force. In this study, AFM was used to measure the surface adhesive force to characterize the adhesion features of the surfaces. The friction force of the surfaces under different loads was measured by continuously increasing the normal load of the probe on the surfaces to obtain the relationship between the friction force and the normal load. The average adhesive force was reported in this study. The linear fitting results of friction force versus normal load (25 nN–250 nN) for surfaces with different adhesion features are shown in Fig. 2. It indicated that the normal load was linearly related to the friction force of the surface, and the adhesive force was the horizontal intercept of the fitting line, i.e., the load when the friction force was zero. Table 2 shows the measurement results, and the adhesive force of 1# was the largest and that of 4# was the smallest, which was consistent with the expectations of the above sample preparation. The adhesive force can be used as a presentation of the adhesion features for surfaces.

2.2 Participants

Ten healthy, 22 to 25 years of age (mean ± standard deviation = 23.8 ± 1.2 years), right-handed males, participated in this study. Before the test, all subjects were requested to provide written informed consent. This study was carried

**Fig. 2** Linear fitting results of the friction force versus the normal load**Table 2** Adhesive force of samples

Samples	1#	2#	3#	4#
Slope	0.74	0.56	0.32	0.19
Vertical intercept	40.33	19.31	6.58	2.35
Adhesive force F_a /nN	54.49	34.48	20.56	12.37

out according to the international ethical standards and was approved by the Ethics Committee of Xuzhou Central Hospital (No. XZXY-LJ-20210513–054).

2.3 Friction Measurement

In this study, a reciprocating motion tribometer was designed for the friction test during the touch process, as shown in Fig. 3a. The index finger touched the silicone samples through the 16×26 mm elliptic hole in the touch stage to ensure a constant contact area. To maintain the stabilization of the touch load and velocity and to keep body from unnecessary motion during the friction process, the samples

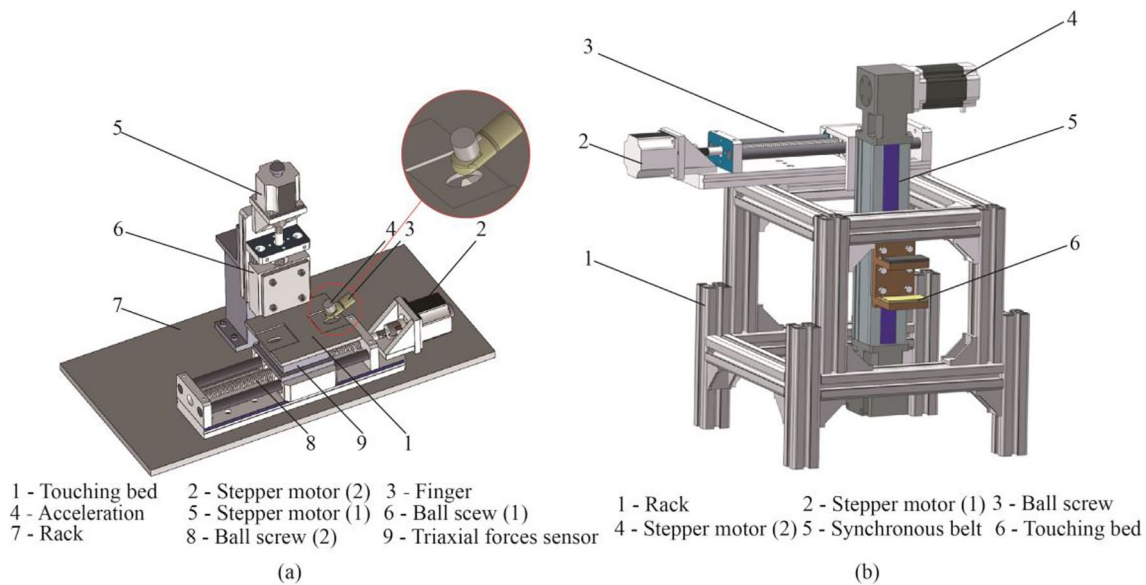


Fig. 3 **a** Structure schematic diagram of the friction test bed **b** Structure schematic diagram of the EEG test bed

were fixed with a double-coating tape on a triaxial force sensor (Bengbu Sensor System Engineering LTD, Bengbu, China) and slid along the surface of the fingers which were kept stationary during the friction test. The normal load and friction force can be measured directly by the triaxial force sensor with force ranges of 0–10 N in the z -direction, 0–5 N in the x - and y -directions and resolutions of 0.2 N and 0.1 N, respectively. Besides, the movement of the sensor was controlled by the ball screw driven by the stepping motor. An acceleration was required and fixed on the nail cap of the index finger to collect the vibration signals in the friction process.

The different touching loads (0.5 N, 1.0 N, 1.5 N, 2.0 N, 2.5 N, and 3.0 N) which can be monitored by the signal acquisition system were applied by participants on the sample surface in the tactile friction test to investigate the influence of adhesion features on the friction component. Then, the touching load of 0.5–0.8 N, touch velocity of 15 mm/s and distance of 45 mm were applied on the surfaces to study the frictional vibrations during the tactile process. All tests were conducted in a laboratory environment with a temperature of 26 to 28 °C and a relative humidity of 45% to 65%.

2.4 ERP Methods

A test bench was designed for the EEG/ERP test to investigate the brain response during the tactile perception, as shown in Fig. 3b. The EEG data in sync with the friction test was recorded using a 32-channel EEG-System (ANT Neuro, Hengelo, Netherlands). Two stepper motors were used to exchange the stimulus sample, accomplishing a

cyclic action of passive touching and return of the sample to its original position. Multiple cyclic actions formed a stimulus sequence. At the onset of touch, a marker signal was sent to the acquisition system, and as the touch ended, another marker signal was also sent to the system. The beginning and end of the tactile EEG signal were determined by these two markers.

An oddball paradigm was used to evoke the ERP components. The two types of stimuli, target and nontarget stimuli were simultaneously required in an oddball paradigm [38]. The nontarget sample appeared 75% of the time, and target samples appeared 25% of the time in this study. The cotton fabric with large differences from silicone samples were selected as the nontarget stimulus and the surfaces with different adhesion features were selected as the target stimulus. Moreover, a pseudorandom sequence was used as the sample test sequence, which was not disclosed to the participants and consisted of a total of 120 stimuli (30 times for the target stimuli and 90 times for the nontarget stimuli). Three stimulus sequences were set up, and one of the sequences was randomly decided before the test to increase the randomness of the stimuli and eliminate the effects of issues such as brain adaptation and self-learning on the tests. A significant ERP waveform can be evoked only when the subjects were actively engaged in the task. Specifically, once the sample surface came into contact with the finger surface, it rubbed against the finger surface for 2.0 s at a constant normal load of approximately 0.5–0.8 N and a touch velocity of 15 mm/s. The interval between each 2 stimuli was 6 s, and the rest period between each set of tests was 10 min.

2.5 Subjective Evaluation

When the subjects contacted the surfaces with different adhesion features, the different adhesive feelings can be perceived. The adhesive evaluation of samples was designed. The dry cotton fabric was initially displayed to subjects as the reference stimulus which perception was set as not adhesive and evaluation scores for adhesion were 0.80-degree and 0-degree liquid silica gels were mixed in a ratio of 1:15 to obtain 5-degree liquid silica gel, which was used to prepare a reference sample. The adhesion evaluation score of the reference sample was defined as 5. The subjects with eyes covered rubbed the sample surface over the skin for 5 s simultaneously. The participants then orally reported the adhesive perceptions of the surfaces, and the range of scores was from 0 to 5. A higher human evaluation score for adhesive sensations corresponded to stronger adhesive feelings, and ultimately, the scores were averaged. Each sample was presented three times per subject.

2.6 Denoising of Vibration Signals

The analysis of vibration frequency spectrum has been widely used in tribological studies [39, 40]. Since the acquired vibration signals inevitably contained the noise from the equipment and environment, the Empirical Mode Decomposition (EMD) method and Independent Component Analysis (ICA) were utilized to remove the noise [41]. The effective signal and the noise signal can be effectively separated using EMD and ICA, which can also reduce the damage to the effective signal during the process of denoising [42]. The vibration signal was decomposed into some Intrinsic Mode Functions (IMFs), which can be used as the

observed signal X_{imf} of ICA. The unmixing matrix V_{rel} was set up, which can be used to transform X_{imf} to obtain the independent source signal S_{ica} . Each component of S_{ica} was correlated with the no-load vibration signals to determine the noise-containing component, which was decomposed once more by EMD to remove the noise to obtain the new independent sources signal S_{ica}' . The denoised IMFs can be obtained by multiplying V_{rel} with S_{ica}' , and the final denoising result was obtained by summing all the IMFs components, as shown in Fig. 4.

2.7 Processing of EEG Signals

In this study, EEGLAB was used to process the EEG data, which were first referenced to an averaged montage of ears. Then, the bandpass was filtered between 0.5 and 40 Hz, and the baseline correction was performed on the data. The EEG data induced by target stimulus were extracted for the analysis of feature extraction. The ERP waveforms were obtained by superimposing and averaging the EEG data for all target stimuli in a single trial. A program was developed in MATLAB to acquire the peak voltage of the ERP waveforms during the 80–120 ms, 180–220 ms, and 280–400 ms time windows selected as the P100, P200, and P300 peak amplitude. The time corresponding to the peak voltage was chosen as the latency. The average peak amplitude and latency of ERP components involved in adhesive perception were calculated.

2.8 NMM of Adhesive Tactile Perception

The NMM is an effective tool to study the brain activity. Compared with real EEG signals obtained from testing,

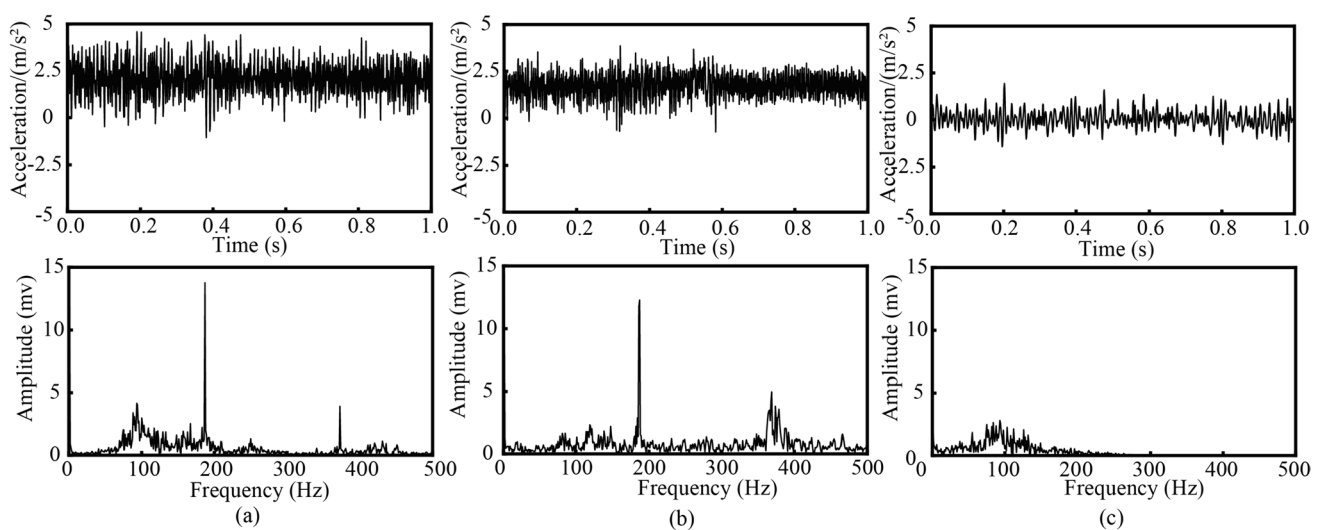


Fig. 4 Typical time-domain signal and frequency spectrum of **a** original vibration signal, **b** no-load vibration signal, and **c** filtered vibration signal

EEG signals simulated by the NMM were not affected by the external noise, and besides, the parameters in the model can be adjusted to directly analyze the physiological responses of the brain induced by the samples with different features. In this study, one-channel NMM was established to investigate the cognitive mechanisms of brain exposed to different tactile stimulus. The principle of the one-channel NMM is shown in Fig. 5.

The one-channel NMM contains two subgroups. Subgroup 1 is composed of pyramidal cells that receive excitatory and inhibitory stimuli from neurons. Subgroup 2 is composed of interneurons, for subgroup 2, the input consists of two parts: the external stimulus $p(t)$, which is replaced by a Gaussian function with a mean $\langle p \rangle$ and a variance σ_p , and the stimuli from the pyramidal cells of subgroup 1. The parameters of V_1 , V_2 , V_3 and V_4 are the numbers of synaptic connections between the pyramidal cells and the interneurons. y_0 represents the output signal of subgroup 1, y_1 and y_2 represent the excitatory and inhibitory output signals of the model, respectively, and y_{out} represents the total output signal of the model.

The dynamic linear transformations are composed of excitatory transformations H_e and inhibitory transformations H_i with the expressions:

$$H_e(t) = \begin{cases} Aate^{-at} & t \geq 0 \\ 0 & t < 0 \end{cases} \quad (2)$$

$$H_i(t) = \begin{cases} Bbte^{-bt} & t \geq 0 \\ 0 & t < 0 \end{cases} \quad (3)$$

where A and B represents the excitatory or slow inhibitory synaptic gain, respectively, and $1/a$ and $1/b$ are the time constants of A and B , respectively.

$S(v)$ represents the static nonlinear transformation in the channel and is an instantaneous function [43]:

$$S(v) = \frac{2e_0}{1 + e^{r(v_0 - v)}} \quad (4)$$

where e_0 represents the maximum firing rate of the neural population, r_0 represents the steepness of the transformation, v_0 represents the postsynaptic potential when the firing rate of the neural population is e_0 , and v represents the average postsynaptic potential.

Therefore, the differential equations that govern the one-channel NMM are as follows:

$$\begin{cases} \dot{y}_0(t) = y_3(t) \\ \dot{y}_3(t) = AaS(y_1(t) - y_2(t)) - 2ay_3(t) - a^2y_0(t) \\ \dot{y}_1(t) = y_4(t) \\ \dot{y}_4(t) = Aa\{p(t) + V_2S(V_1y_0(t))\} - 2ay_4(t) - a^2y_1(t) \\ \dot{y}_2(t) = y_5(t) \\ \dot{y}_5(t) = Bb\{V_4S(V_3y_0(t))\} - 2by_5(t) - b^2y_2(t) \end{cases} \quad (5)$$

In this paper, $\sigma_p = 30$, $y_{out} = y_1(t) - y_2(t)$, $1/a = 1/b = 0.02$ s, $e_0 = 2.5$ s⁻¹, $r_0 = 0.56$ mV⁻¹, and $v_0 = 6$ mV. By modifying the A/B to simulate the excitatory and inhibitory feedback of the brain to tactile perceptions, and adjusting the mean $\langle p \rangle$ of Gaussian function $p(t)$ to simulate the intensity of external tactile stimuli, the variations in the output of the model were observed to study the neurophysiological response of the brain activity exposed to perceptions of different adhesion features.

The EEG rhythm represents different mechanisms of neuronal activity during cognitive processes, while one-channel NMM is difficult to simulate the complex changes in multiple EEG rhythms. Moreover, it is well known that neural masses in the brain are coupled and connected to each other, therefore, two-channel and three-dynamic NMM was established to further reveal the specific information transmission and brain activity between the neural masses during the adhesive tactile perception. The principle of the two-channel NMM is shown in Fig. 6.

The interaction between two populations of neurons is simulated by taking the output of one channel as the input of the other channel. Thus, the input to channel 2 consists of two parts: the external stimulus $p(t)$ and the input from channel 1 to channel 2, $S(y_1(t-\delta))$. The deviation of $p(t)$ may decrease to $1-k_{12}$ times that of the original (k_{12} is the connectivity constant of channel 1 to channel 2, $0 \leq k_{12} \leq 1$) due to the input of channel 1. To keep the standard deviation of the total model input constant, the parameter k_{12}^* is needed. Due to $\langle \tilde{p}_2 S(y_1) \rangle = 0$, the value of k_{12}^* can be derived from:

$$k_{12}^* = \frac{\sigma_{p_2} \sqrt{2k_{12} - k_{12}^2}}{\sigma_{S(y_1)}} \quad (6)$$

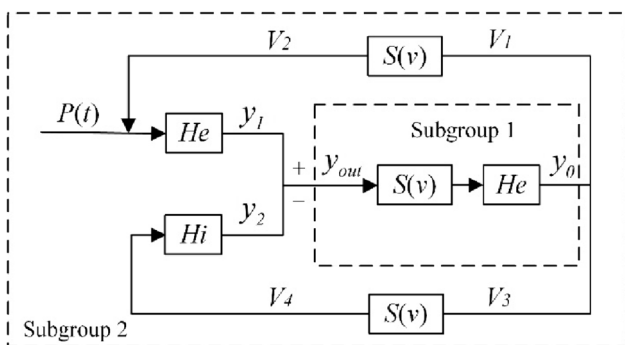


Fig. 5 Principle of one-channel NMM

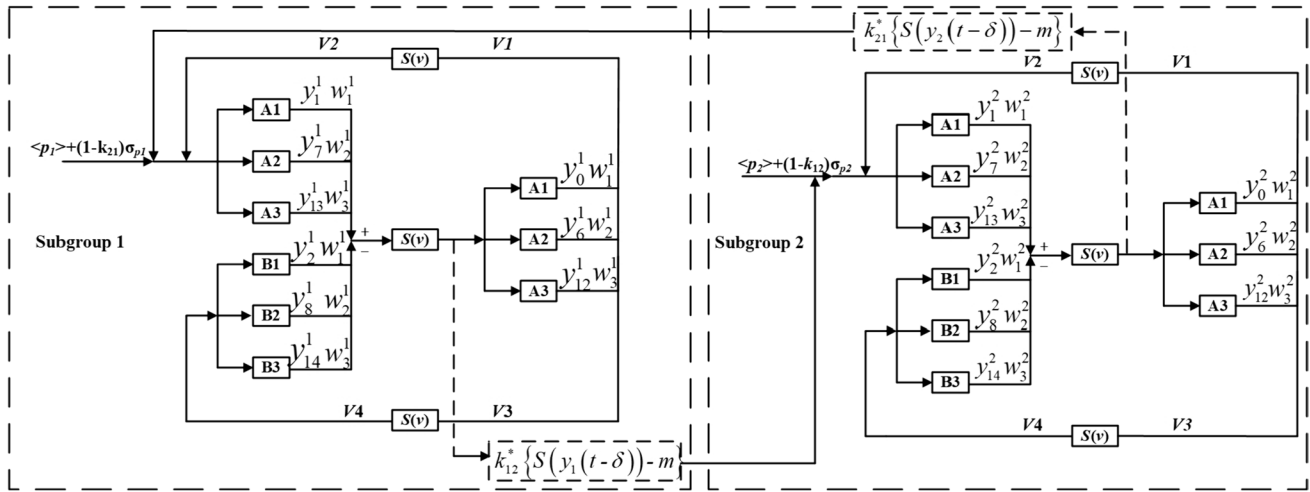


Fig. 6 Schematic diagram of the two-channel NMM

Each channel in the model contains three dynamics, one of which represents a subgroup, and different parameters are used to generate simulation signals of different rhythms. w_n is used to represent the weight of each dynamic signal in the total signal of the channel, $0 \leq w_n \leq 1$, and its sum is 1. The EEG rhythm generated by the channel simulation signals can be adjusted to produce more rhythmically abundant signals by adjusting the weight coefficient [w_1, w_2, w_3]. The standard settings of typical rhythms were used in this model, which can generate δ, α and γ rhythms. The parameter settings are shown in Table 3 [44]. The sampling period of the model was 0.001 s, the mean value of $p(t)$ was $\langle p \rangle = 30$, the variance $\sigma_p = 30$, and the time delays were 10 ms.

According to the principle of the NMM, the differential equation of this model can be obtained. The equations are similar for all dynamics, taking one of the dynamics as an example:

3 Results and Discussions

3.1 Friction Analysis between Skin and Samples with Different Surface Adhesion

It is well known that the skin is a viscoelastic material, and the friction between the finger surface and the sample surfaces mainly composed of the adhesive friction F_s and the deformation friction F_d . The friction coefficient and the friction force of the skin are governed by the following relationships [17, 45]:

$$F_s = \tau A_s = \pi \tau_0 \left(\frac{3R}{4E} \right)^{\frac{2}{3}} W^{\frac{2}{3}} + \xi w \tag{8}$$

$$\left\{ \begin{array}{l} \dot{y}_0^1(t) = y_3^1(t) \\ \dot{y}_3^1(t) = A_1 a_1 S \left(\begin{array}{l} w_1^1 y_1^1(t) + w_2^1 y_7^1(t) + w_3^1 y_{13}^1(t) \\ -w_1^1 y_2^1(t) - w_2^1 y_8^1(t) - w_3^1 y_{14}^1(t) \end{array} \right) - 2a_1 y_3^1(t) - (a_1)^2 y_0^1(t) \\ \dot{y}_1^1(t) = y_4^1(t) \\ \dot{y}_4^1(t) = A_1 a_1 \left\{ \begin{array}{l} k_{21}^* \left[S \left(\begin{array}{l} w_1^2 y_1^2(t) + w_2^2 y_7^2(t) + w_3^2 y_{13}^2(t) \\ -w_1^2 y_2^2(t) - w_2^2 y_8^2(t) - w_3^2 y_{14}^2(t) \end{array} \right) - m \right] \\ + \langle p_1 \rangle + (1 - k_{21}) \sigma_{p1} \\ + V_2 S(V_1 (w_1^1 y_0^1(t) + w_2^1 y_6^1(t) + w_3^1 y_{12}^1(t))) \end{array} \right\} - 2a_1 y_4^1(t) - (a_1)^2 y_1^1(t) \\ \dot{y}_5^1(t) = y_5^1(t) \\ \dot{y}_5^1(t) = B_1 b_1 \{ V_4 S(w_1^1 y_0^1(t) + w_2^1 y_6^1(t) + w_3^1 y_{12}^1(t)) \} - 2b_1 y_5^1(t) - (b_1)^2 y_2^1(t) \end{array} \right. \tag{7}$$

Table 3 Standard parameters for the three rhythms

Parameters	Standard parameters of rhythms		
	δ	α	γ
Average gain of excitatory synapse /mV	2	3.25	7.5
Average gain of slow inhibitory synapse /mV	15	22	150
Time constant of excitatory feedback circuits /s	0.05	0.0108	0.0046
Time constant of slow inhibitory feedback circuits /s	0.05	0.02	0.0029

$$F_d = \beta_{los} \left(\frac{9}{128R} \right)^{\frac{2}{3}} \left(\frac{1 - p_r^2}{E} \right)^{\frac{1}{3}} W^{\frac{4}{3}} \tag{9}$$

$$\mu = \frac{F}{W} = kW^{n-1} \tag{10}$$

where τ represents the interfacial shear strength, A_s represents the real contact area, W is the normal load, τ_0 represents the intrinsic interfacial shear strength, R is the radius of the sphere, ξ is a pressure coefficient, E and P_r are the Young’s modulus and Poisson’s ratio of skin, β_{los} is the viscoelastic hysteresis loss fraction, k is a load-dependent friction coefficient, and n is the load index. With reference to Eqs. (8) and (9), it can be noticed that the adhesive friction corresponds to a load index n of 2/3 and the deformation friction corresponds to a load index n of 4/3. In this study, the friction tests at different normal loads were carried out, and the friction coefficients as a function of different applied normal loads for all surfaces are shown in Fig. 7. Furthermore, the friction data were fitted according to Eq. (10), and the results of k and n are reported in Table 4.

It indicated that the load index decreased as the surface adhesion increased, indicating that the adhesive friction component gradually increased, and the deformation friction component gradually decreased. The results also showed that the friction coefficient of samples 1# and 2# decreased with the increasing normal load, and the values of n were 0.75 and 0.83, respectively, which were approaching the load index of adhesive friction. It suggested that the adhesive friction was dominant as fingers slid over samples 1# and 2#. The variation trend of the friction coefficient of samples 3# and 4# was not significant with the varied normal load, and the load index n was 0.94 and 1.05, respectively, which was close to 1, indicating that the friction between samples 3# and 4# and fingers was affected by the combination of adhesive friction and deformation friction. In this case, as the touching load varied, variations of two friction component counteracted each other, resulting in insignificant changes in friction coefficient.

Table 4 Experimental and derived data of the four samples

Samples	1#	2#	3#	4#
k	1.70	1.28	0.85	0.70
n	0.75	0.83	0.94	1.05

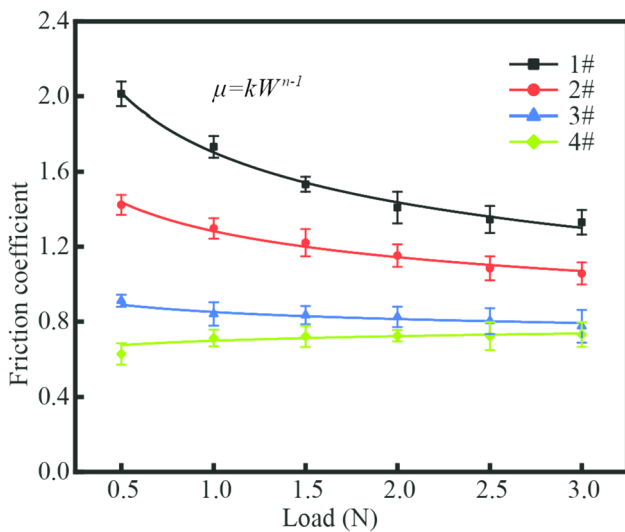


Fig.7 Friction coefficient as a function of applied load for four samples

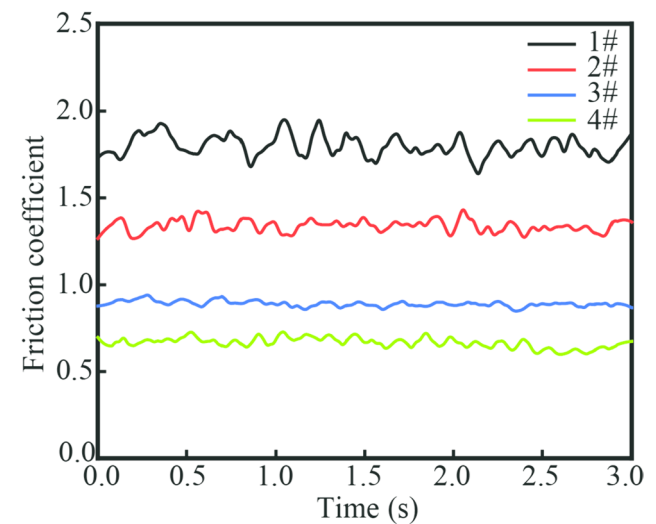


Fig.8 Friction coefficient of finger touching surfaces with different adhesion features

3.2 Correlation of Friction and Vibration Features with Adhesive Perception

Figure 8 shows the typical friction coefficient curves of a finger touching the surfaces with different adhesion features at a touch load of approximately 0.5–0.8 N. The results showed that the fluctuation of the friction coefficient curves became smaller as the surface adhesion decreased. The fluctuation of the friction coefficient curve of sample 1# was the most obvious, and showed the typical sawtooth characteristics of the stick–slip phenomenon, which is mainly attributed to the properties of silicone. First, due to the larger adhesive force of the surface, the static friction of the interface at this time was significantly greater than the kinetic friction, so the friction coefficient increased. During the touching process, the elastic deformation of the sample gradually occurred, and the deformation increased with the relative movement between the sample and the finger. When the deformation increased to the point where the deformation recovery force can overcome the static friction, the deformation of the sample recovered, and the friction coefficient decreased. Then, elastic deformation occurred again, and this stick–slip process was repeated during the touching process.

Furthermore, the variations in the friction coefficient, adhesive perception, and vibration amplitude with respect

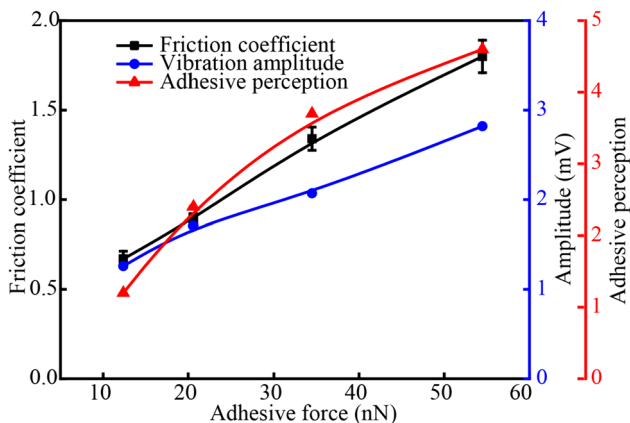
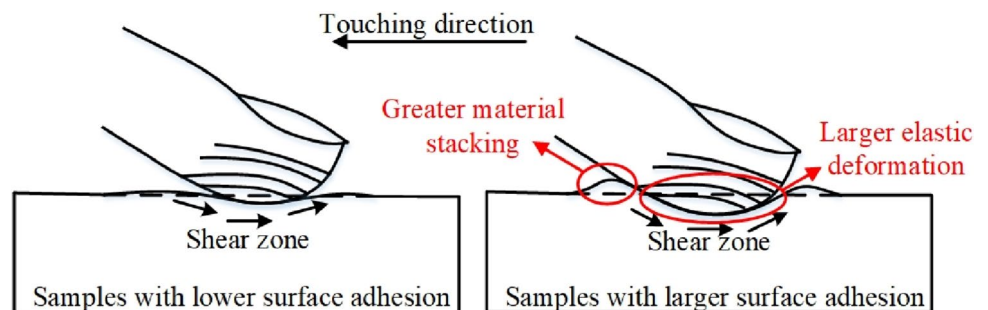


Fig. 9 The relationship between adhesive force, friction coefficient, vibration amplitude, and adhesive perception

Fig. 10 Schematic diagram of a finger touching adhesive surfaces



to the surface adhesive force are shown in Fig. 9. Pearson correlation analyses were utilized to evaluate the correlation of the friction coefficient μ , the adhesive perception, and the vibration amplitude with the adhesive force. In Pearson correlation analysis, the correlation coefficient r indicates the linear correlation between two variables, and the p -value indicates the statistical significance of the correlation coefficient. The results showed that μ and adhesive perception were positively correlated with the adhesive force, with $r=0.997$ and $p=0.003$ and $r=0.969$ and $p=0.031$, respectively. This is mainly due to the intermolecular attractive force between the finger and the adhesive surface increased with the increasing surface adhesion. The contact area and adhesive friction component between the finger and surfaces increased due to the increase in the adhesive force and the decrease in hardness of samples, and as a result, the average friction coefficient and adhesive perception increased.

The results also showed that the vibration amplitude was positively correlated with the adhesive force with $r=0.997$ and $p=0.003$. During the touching process, the elastic deformation in the normal direction was constantly generated and then recovered due to the occurrence of stick–slip behavior, at the same time, the process of energy storage and release was caused by material stacking and recovery in the friction direction, respectively. The elastic deformation and the stack of the material played important roles in the vibration amplitude. With the increasing surface adhesion, the elastic modulus decreased and the stick–slip phenomenon became more obvious, and as a result, the elastic deformation and the stack of the materials increased, as shown in Fig. 10. Therefore, the energy involved in the friction process and the vibration amplitude increased with the increasing adhesion of surfaces.

The friction coefficient μ and vibration amplitude were positively correlated with the adhesive perception with $r=0.981$ and $p=0.019$ and $r=0.973$ and $p=0.027$. It indicated that the larger the friction coefficient and the larger the vibration amplitude, the stronger the adhesion feeling was.

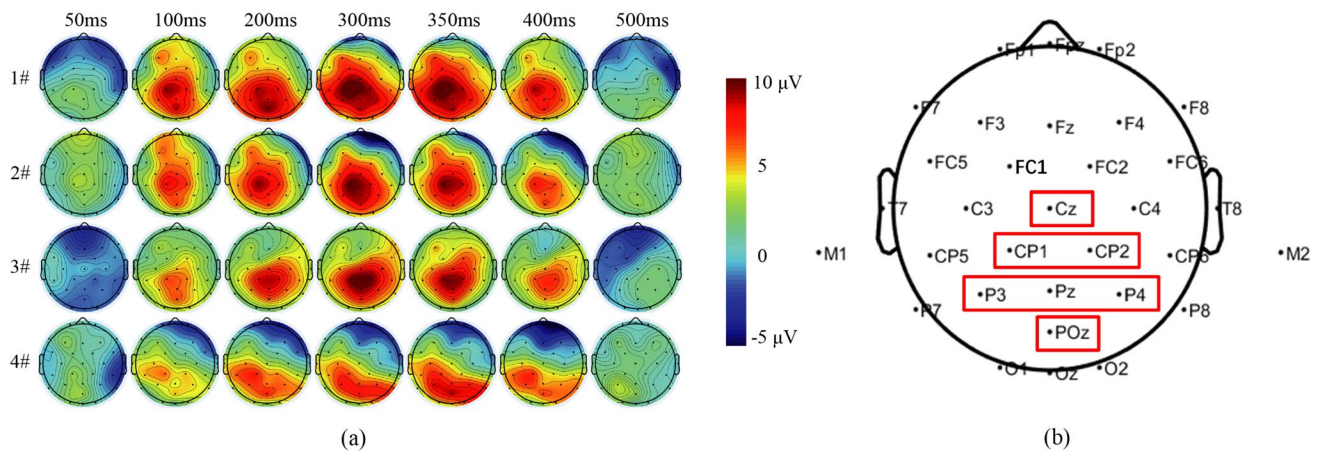


Fig. 11 **a** Average ERP scalp maps of four samples **b** Location distribution of 32 channels of electrodes

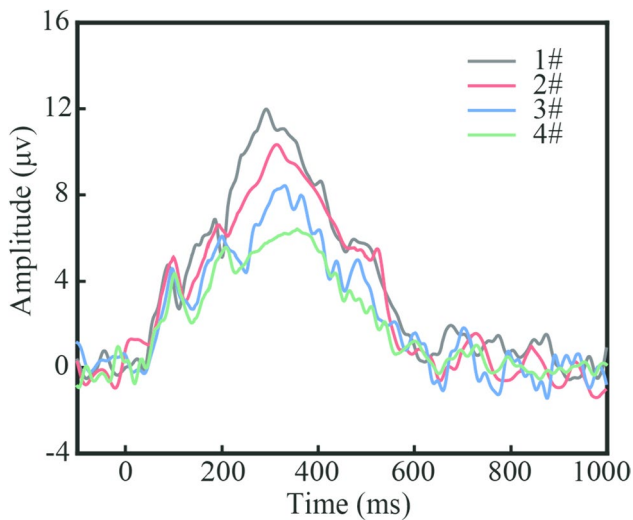


Fig. 12 Average ERP waveform of four samples

3.3 EEG Analysis of Adhesive Perception

Figure 11 shows the average ERP scalp maps of four samples with different adhesion features, which can reflect the area and intensity of brain activity. The color of ERP scalp maps changes from blue to red to represent a change in voltage from low to high. It demonstrated that the parietal lobe and occipital lobe areas were positively activated, and the active brain area and activation intensity increased with the increasing surface adhesion. During tactile perception, the amplitude of the ERP scalp maps gradually increased and reached its maximum between 300 and 350 ms and then gradually decreased after 350 ms. At the time window of 500 ms, the amplitude was close to the prestimulation value, indicating that the processing of tactile perception of adhesion was completed by the brain at this time.

Table 5 Latency and amplitude of three components of ERP

Samples	Latency (ms)/Amplitude (μ V)		
	P100	P200	P300
1#	89 ^a /4.76 ^a	185 ^a /6.83 ^a	293 ^a /11.97 ^a
2#	100 ^a /5.14 ^a	192 ^a /6.59 ^a	314 ^b /10.33 ^b
3#	98 ^a /4.60 ^a	201 ^b /6.08 ^b	329 ^c /8.41 ^c
4#	102 ^a /4.37 ^a	207 ^b /5.54 ^c	356 ^d /6.53 ^d

Note: Means marked with different letters in the same column are significantly different from each other and means marked with the same letter are not significantly different from each other ($P < 0.05$)

As shown in Fig. 11, Cz, CP1, CP2, P3, Pz, P4, and POz electrodes were selected for further study because the parietal lobe and occipital lobe areas of the brain were involved in adhesive perception. The average ERP waveforms of the chosen electrodes are shown in Fig. 12. The difference between the mean prestimulus baseline voltage and the ERP waveform's largest positive-going peak within a time window is referred to as the amplitude [46]. The time between the beginning of the stimulus and peak positive amplitude within a time window is known as the latency. The mean latency and amplitude of induced components of ERP are shown in Table 5. It suggested that P100 and P200, and P300 were successfully evoked during tactile perception for all surfaces. There were no significant differences in the P100 component evoked by the four surfaces. It suggested that the P200 amplitude evoked by samples 1# and 2# had no significant differences but compared with the samples 3# and 4#, significant differences were observed, and the P200 amplitude decreased with the decreasing adhesive force.

The P300 component of ERP is a typical endogenous component elicited in the decision-making process and reflects the basic cognitive processes. Based on the references [30, 47], the P300 amplitude is proportionally related

to the number of attentional resources involved in processing a given stimulus. The P300 latency reflects the speed of volunteers' judgment for surfaces with different features and correlates with the difficulty of the test [48]. Thus, the P300 component was used as an electrophysiological characterization of adhesive perception in this study. As shown in Table 5, the P300 latency was significantly negatively correlated with the adhesive force with $r = -0.965$ and $p = 0.035$,

Table 6 Intensity of brain activation results of EEG source localization

Samples	1#	2#	3#	4#
Intensity of brain activation	37.9	31.0	20.8	14.4

indicating that more time was needed by surfaces with lower adhesion in the adhesive perception judgment. The results showed that the P300 amplitudes were significant differences among the four samples, and the P300 amplitudes decreased with the decreasing surface adhesion. The P300 amplitudes were significantly positively correlated with the adhesive force with $r = 0.991$ and $p = 0.009$, indicating that more attentional resources were required for surfaces with larger adhesion in the perception judgment. During the touching process, as the surface adhesion increased, the coefficient of friction and the frictional vibrations of the skin against a surface increased, leading to larger stimulation of the tactile receptors beneath the finger skin, and as a result, the intensity of the neurophysiological response increased and more

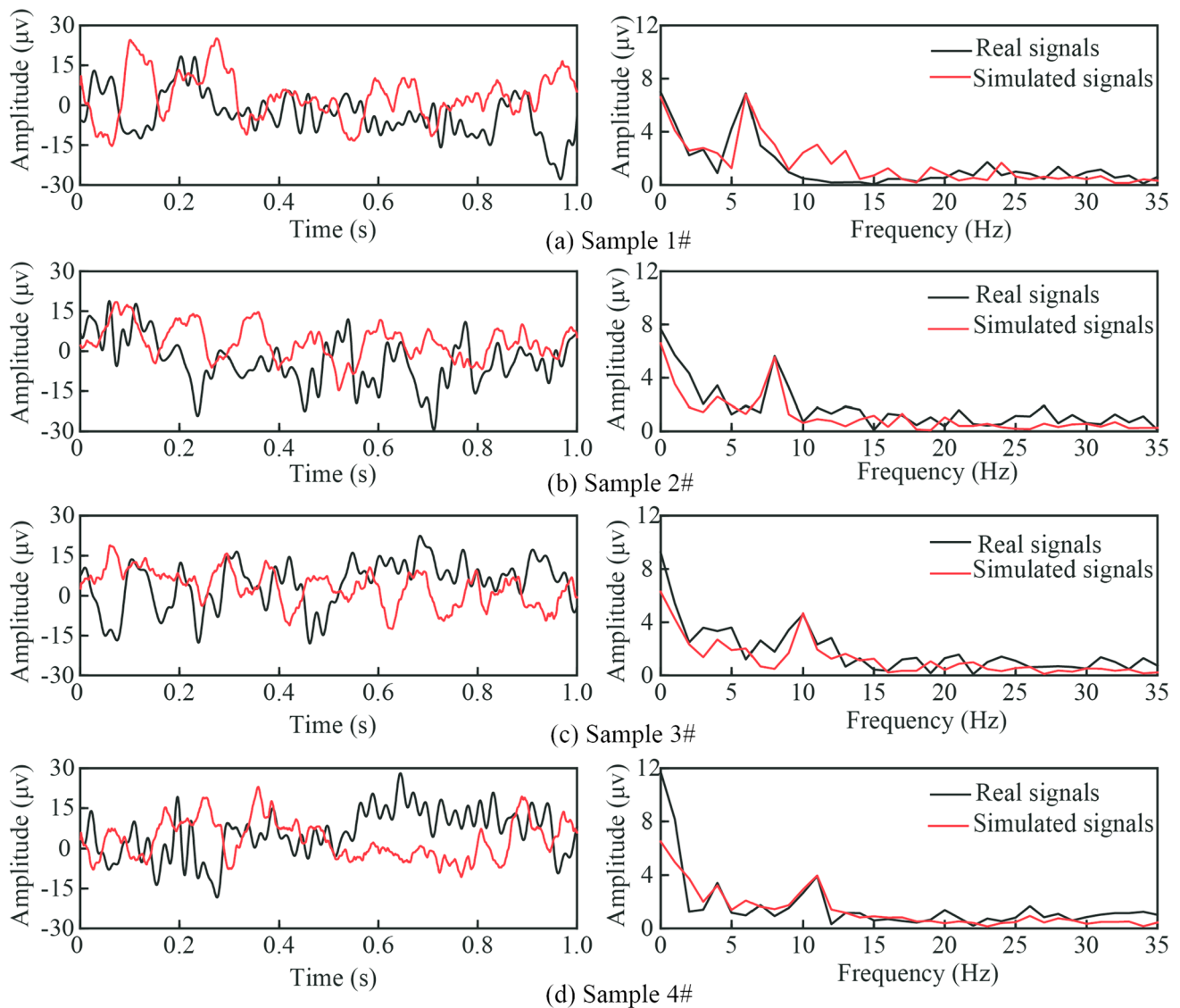


Fig. 13 Comparison of one-channel simulated and real EEG signals

Table 7 Frequency and amplitude of real EEG and one-channel simulated signals

Signals	1#	2#	3#	4#
Dominant frequency (Hz)/ Amplitude (μV) of real signals	6/6.90	8/5.64	10/4.59	11/3.92
$\langle p \rangle / A/B$	38.1/0.137	27.9/0.092	17.2/0.038	11.8/0.012
Dominant frequency (Hz)/ Amplitude (μV) of simulated signals	6/6.82	8/5.56	10/4.69	11/3.97

attentional resources were involved in the tactile perception for surfaces with larger adhesion.

Furthermore, the EEG signals at the time points corresponding to the latency of the P300 component were used for EEG source localization to obtain the intensity of brain activity induced by surfaces with different adhesion features. As shown in Table 6, it demonstrated that the activation intensity of the brain was significantly positively correlated with the adhesive force, with $r=0.981$ and $p=0.019$, indicating the intensity of brain activation and attentional resources involved increased with the increasing adhesive force.

3.4 EEG Signals Simulated by NMM

Figure 13 shows the comparison between the real and simulated EEG signals excited by the surfaces with different adhesion features. Table 7 shows the dominant frequency and amplitude of the real and simulated EEG signals. A mean $\langle p \rangle$ of $p(t)$ represents the average intensity of external tactile perception, and A/B is the ratio of the excitatory or slow inhibitory synaptic gain, which can be used to represent the excitatory and inhibitory feedback of the brain response. Correlation analysis was performed on the spectrum of the real and the simulated EEG signals, and there was a significant correlation with $p=0.001$ and $r=0.858$, indicating that the EEG signals induced by surfaces with different adhesion features can be simulated by adjusting the mean $\langle p \rangle$ and A/B in the model.

Table 8 Frequency and amplitude of simulated signals with different $\langle p \rangle$

Signals	Signal 1	Signal 2	Signal 3	Signal 4
$\langle p \rangle$	38.1	27.9	17.2	11.8
Dominant frequency (Hz) / Amplitude (μV) of simulated signals	6/6.8	6/5.5	6/4.6	6/3.9

Table 9 Frequency and amplitude of simulated signals with different A/B

Signals	Signal 1	Signal 2	Signal 3	Signal 4
A/B	0.137	0.092	0.038	0.012
Dominant frequency (Hz)/ Amplitude (μV) of simulated signals	6/6.79	8/6.75	10/6.82	11/6.81

The influence of surface with different adhesion features on the brain activity was investigated by keeping $A/B=0.137$ and increasing the mean $\langle p \rangle$. It can be seen from Table 8, the dominant frequency of simulated EEG signals was not affected by the mean $\langle p \rangle$, but the amplitude decreased with the decrease of $\langle p \rangle$, which was consistent with the results of real EEG signals in Table 7. It suggested that the amplitude of simulated EEG signals and the intensity of adhesive tactile perceptions increased with the increasing surface adhesion. This result was in agreement with the above result obtained from the EEG source localization, indicating that the activation intensity of the brain increased for the surfaces with larger adhesion.

The excitability of brain response to the surfaces with different adhesion features was studied by keeping the $\langle p \rangle = 38.1$ and decreasing the A/B . Table 9 shows the dominant frequency and amplitude of simulated EEG signals. It indicated that the dominant frequency of simulated EEG signals increased with the decrease of A/B , which was consistent with the variations of real EEG signals. The results demonstrated that as the surface adhesion increased, the excitability of brain response increased and the dominant frequency decreased.

To further reveal the specific information transmission and brain activity between the neural masses during the tactile perception of surfaces with different adhesion features, the EEG signals were simulated using the two-channel and three-dynamic NMM. Figure 14 shows the comparison between the real EEG signals and the simulated EEG signals excited by the two-channel and three-dynamic NMM. Table 10 shows the dominant frequency and amplitude of the real and simulated EEG signals. Due to the same parameter settings for the simulation, the outputs of both channels were almost identical, and therefore, the simulated EEG signal output from channel 1 were compared with the real EEG signals. It may be seen that the simulated EEG signals similar to real signals in the frequency domain can be obtained by adjusting the weight coefficient [w_1, w_2, w_3] of the three dynamics as well as the connectivity constant k_{12} and k_{21} between the two channels. Correlation analysis was performed on the spectrum of the real EEG signals and the simulated signals, and there was a significant correlation with $p=0.001$ and $r=0.842$, indicating that the real EEG signals can be simulated using the two-channel and

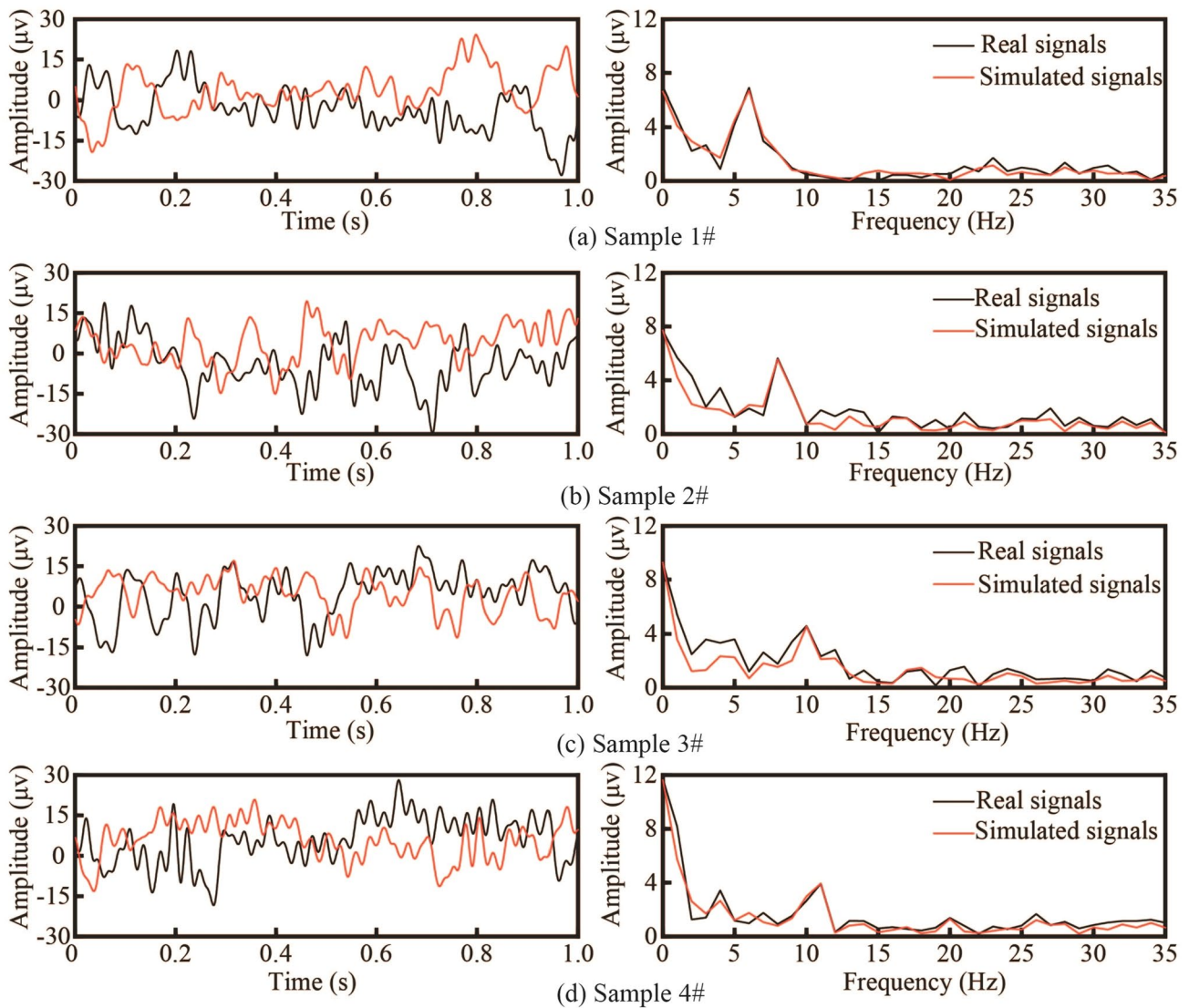


Fig. 14 Comparison of real EEG signals and simulated signals

Table 10 The dominant frequency and amplitude of real signals and simulated EEG signals

Signals	1#	2#	3#	4#
Dominant frequency (Hz)/ Amplitude (µV) of real signals	6/6.89	8/5.63	10/4.59	11/3.92
Weight coefficient ($w_1/w_2/w_3$)	0.50/0.37/0.13	0.44/0.41/0.14	0.34/0.54/0.12	0.31/0.59/0.10
Connectivity constant k_{12}/k_{21}	0.35/0.35	0.26/0.26	0.17/0.17	0.14/0.14
Dominant frequency (Hz)/ Amplitude (µV) of simulated signals	6/6.71	8/5.57	10/4.56	11/3.93

Table 11 The dominant frequency and amplitude of simulated signals with different weight coefficients

Simulated signals	Signal 1	Signal 2	Signal 3	Signal 4
Weight coefficient ($w_1/w_2/w_3$)	0.50/0.37/0.13	0.44/0.41/0.14	0.34/0.54/0.12	0.31/0.59/0.10
Dominant frequency (Hz)/Amplitude (µV) of simulated signals	6/5.59	8/5.51	10/5.63	11/5.55

Table 12 The dominant frequency and amplitude of simulated signals with two-way connectivity

Simulated signals	Signal 1	Signal 2	Signal 3	Signal 4
Connectivity constant k_{12}/k_{21}	0.35/0.35	0.26/0.26	0.17/0.17	0.14/0.14
Dominant frequency (Hz)/Amplitude (μV) of simulated signals of channel 1	6/6.93	6/5.69	6/4.69	6/3.89
Dominant frequency (Hz)/Amplitude (μV) of simulated signals of channel 2	6/6.91	6/5.67	6/4.65	6/3.94

three-dynamic NMM. Besides, in the band of low frequency, the EEG signals simulated by the two-channel NMM was more similar to the real signals than that simulated by the one-channel NMM.

The weight coefficients $[w_1, w_2, w_3]$ can be used as representations of the effects of the signals generated by different dynamics on the EEG rhythm, and the larger the coefficients are, the larger the effect on the simulated signals. As the connectivity constant $k_{12} = k_{21} = 0$, the effects of the weight coefficients $[w_1, w_2, w_3]$ on the signals were studied, and the results are shown in Table 11. The two channels of the NMM were independent at this time. Therefore, only the simulation results of channel 1 are displayed. It can be found that the weight coefficient w_1 decreased and w_2 increased with the decreasing of the surface adhesion, but no significant difference was observed in the weight coefficient w_3 . The dominant frequency of the simulated signals gradually increased with decreasing surface adhesion, which is consistent with the real EEG signals. It demonstrated that as the surface adhesion decreased, the effects of the δ rhythm on the dominant frequency of the EEG signals decreased, and the effects of the α rhythm on the dominant frequency of the EEG signals increased.

The connectivity direction of the two-channel and three-dynamic NMM represents the direction of transmission of EEG signals, and the connectivity constant represents the relatedness and the intensity of information transmission between the two channels. The two-way connectivity between two channels represents mutual information transmission between two neural masses. In this case, the model can be used to present the central location of the brain area activated by adhesive perception, and the connectivity strength can be used as a presentation of the activation intensity. The weight coefficients were kept constant and the connectivity constant k_{21} ($k_{12} = k_{21}$) was varied to investigate the variation in EEG signals during the transmission of adhesive tactile information between the two neural masses. Table 12 shows the dominant frequency and the amplitudes of simulated signals

obtained by adjusting the connectivity constant. As the connectivity constant decreased, the amplitudes of signals simulated by two channels decreased, and the difference in the amplitudes between the two channels was not significant, which was consistent with the rule of the variation of real EEG signals. It is indicated that the connectivity strength between the two neural masses, the intensity of brain activity, and the amplitudes of EEG signals increased with increasing surface adhesion.

The fluctuations of EEG signals represent different mechanisms of neuronal activity during cognitive processes. In this study, in the presence of tactile stimulus with different adhesion features, the EEG signals can be simulated effectively by both the one-channel and two-channel NMM. The connectivity strength and the tactile information transmission between the two neural masses, as well as the excitability and activity intensity of the brain response to adhesive surfaces can be systematically investigated through the NMM, contributing to a further comprehension of the neurophysiological mechanisms of adhesive perception.

4 Conclusions

This study systematically studied adhesive perception based on a subjective evaluation, skin friction and vibration, and the brain activity. The NMM was established to investigate the production mechanisms of adhesive perception. The study found that the features of the friction coefficient and vibration amplitude were positively correlated with the perceived adhesion. The parietal lobe and occipital lobe were engaged in the adhesive tactile perceptions of silicone samples, and less time and more attentional resources were involved in the perception of samples with larger surface adhesion. One-channel NMM revealed that as the surface adhesion and the intensity of external tactile stimuli increased, the dominant frequency of EEG signals decreased, and the excitability and intensity of the brain activity increased. The two-channel NMM further demonstrated that the connectivity strength between the two neural masses increased with the increasing surface adhesion. This study is significant for understanding the frictional behavior between soft silicone materials and skin surfaces and the role of surface adhesion in tactile perception. It is also of great significance to enhance the perceived comfort and the grip reliability of skin-touch products such as prosthetic sockets, handles of labor and sporting goods, anti-slip pads, and phone cases. Furthermore, the influence of surface texture, touching velocity, individual differences (age, gender, and fingerprint) on tactile sensation can be carried out to study the adhesive tactile perception systematically.

Acknowledgements The authors acknowledge financial support from the National Natural Science Foundation of China (Nos. 52375224 and 51875566) and A Project Funded by the Priority Academic Program Development of Jiangsu Higher Education Institutions.

Funding The National Natural Science Foundation of China, 52375224, Tang Wei, 51875566, Tang Wei, Priority Academic Program Development of Jiangsu Higher Education Institutions.

Data Availability The authors declare that the data supporting the findings of this study are available within the paper.

Declarations

Conflict of interest The authors declare no conflict of competing or financial interests in this work.

References

- Wu, A., Zhang, Z., Shi, X., & Liu, C. (2023). Modeling the role of interfacial adhesion in the rolling resistance of a hyperelastic wheel. *Tribology International*, *185*, 108494.
- Ciavarella, M., Joe, J., Papangelo, A., & Barber, J. R. (2019). The role of adhesion in contact mechanics. *Journal of the Royal Society Interface*, *16*(151), 20180738.
- Dangnan, F., Espejo, C., Liskiewicz, T., Gester, M., & Neville, A. (2020). Friction and wear of additive manufactured polymers in dry contact. *Journal of Manufacturing Processes*, *59*, 238–247.
- Yuan, J. Y., Zhang, Z. Z., Yang, M. M., Li, P. L., Zhao, X., & Wang, W. J. (2022). Adopting bio-inspired interfacial modification and reinforcements simultaneously for optimizing the tribological performance of fabric composites. *Tribology International*, *169*, 107495.
- Chen, D. H., Yang, X., Zhong, M. H., Chen, C., Wang, L. H., Wang, J. C., Weng, X. H., Li, Y. W., & Chang, Z. Y. (2022). Inspired by tree frog: Bionic design of tread pattern and its wet friction properties. *Journal of Bionic Engineering*, *19*(4), 1064–1076.
- Wang, Z. Y., Xing, Q., Wang, W. B., Ji, A. H., & Dai, Z. D. (2018). Contribution of friction and adhesion to the reliable attachment of a gecko to smooth inclines. *Friction*, *6*(4), 407–419.
- Hu, H., Wang, D. R., Tian, H. M., Huang, Q. Y., Wang, C. H., Chen, X. L., Gao, Y., Li, X. M., Chen, X. M., Zheng, Z. J., & Shao, J. Y. (2022). Bioinspired hierarchical structures for contact-sensible adhesives. *Advanced Functional Materials*, *32*(8), 2109076.
- He, Q. S., Zhao, Z. F., Zhang, H., Duan, J. J., Zhang, N., Cui, K. K., Zhong, Q. Y., & Yang, C. L. (2021). Bioinspired adhesive manufactured by projection microstereolithography 3D printing technology and its application. *Advanced Materials Interfaces*, *10*(14), 2202465.
- Li, R. Z., Li, D. W., Sun, J., Zhang, X. L., & Zhang, W. M. (2023). Pull-off dynamics of mushroom-shaped adhesive structures. *Journal of the Mechanics and Physics of Solids*, *183*, 105519.
- Wang, W., Liu, Y., & Xie, Z. W. (2021). Gecko-like dry adhesive surfaces and their applications: A review. *Journal of Bionic Engineering*, *18*(5), 1011–1044.
- Mergel, J. C., Scheibert, J., & Sauer, R. A. (2021). Contact with coupled adhesion and friction: Computational framework, applications, and new insights. *Journal of the Mechanics and Physics of Solids*, *146*, 104194.
- Zhang, J. Y., Tian, H. M., Liu, H. R., Wang, D. R., Wu, Y. H., Li, X. M., Wang, C. H., Chen, X. L., & Shao, J. Y. (2023). Electro-thermal dry adhesives with high adhesion under low temperatures based on tunable stiffness. *Advanced Functional Materials*, *2023*, 2309800.
- Zi, P., Xu, K., Tian, Y. B., & Ding, X. L. (2023). A mechanical gripper inspired by beetle claw for a rock climbing robot. *Mechanism and Machine Theory*, *181*, 105168.
- Li, L. Z., Liu, Z. Y., Zhou, M., Li, X. X., Meng, Y. G., & Tian, Y. (2019). Flexible adhesion control by modulating backing stiffness based on jamming of granular materials. *Smart Materials and Structures*, *28*(11), 115023.
- Li, X. S., Bai, P. P., Li, X. X., Li, L., Li, Y. Z., Lu, H. Y., Ma, L. R., Meng, Y. G., & Tian, Y. (2022). Robust scalable reversible strong adhesion by gecko-inspired composite design. *Friction*, *10*(8), 1192–1207.
- Li, X. S., Li, X. X., Li, L., Sun, T. H., Meng, Y. G., & Tian, Y. (2021). Trumpet-shaped controllable adhesive structure for manipulation of millimeter-sized objects. *Smart Materials and Structures*, *30*(11), 115003.
- Adams, M. J., Briscoe, B. J., & Johnson, S. A. (2007). Friction and lubrication of human skin. *Tribology Letters*, *26*(3), 239–253.
- Tomlinson, S. E., Carré, M. J., Lewis, R., & Franklin, S. E. (2011). Human finger contact with small, triangular ridged surfaces. *Wear*, *271*(9–10), 2346–2353.
- Gao, Y. L., & Wang, Y. J. (2023). Research on the dynamic behaviors in the sliding friction of silicone. *Tribology Letters*, *71*(1), 15.
- Augurelle, A. S., Smith, A. M., Lejuune, T., & Thnnord, J. L. (2003). Importance of cutaneous feedback in maintaining a secure grip during manipulation of hand-held objects. *Journal of Neurophysiology*, *89*(2), 665–671.
- Golden, R. M. (2002). Spiking interest in computational modeling: A unified approach to cognitive neuroscience. Review of computational explorations in cognitive neuroscience: Understanding the mind by simulating the brain. *Journal of Mathematical Psychology*, *46*(5), 636–653.
- Childs, T. H. C., & Henson, B. (2007). Human tactile perception of screen-printed surfaces: Self-report and contact mechanics experiments. *Proceedings of the Institution of Mechanical Engineers, Part J: Journal of Engineering Tribology*, *221*(J3), 427–441.
- Y Muramatsu M Niitsuma 2013 Correspondence relationships between vibrotactile stimuli and tactile sensations determined by semantic differential. In Proceedings-ieee international workshop on robot and human interactive communication: (iecc), Gyeongju, Korea, 668–673.
- Tang, W., Chen, N. X., Zhang, J. K., Chen, S., Ge, S. R., Zhu, H., Zhang, S. G., & Yang, H. F. (2015). Characterization of tactile perception and optimal exploration movement. *Tribology Letters*, *58*(2), 28.
- Mith, S., Carpentier, L., & Monteil, G. (2008). Correlation between the sensorial perception and the descriptive instrumental analysis of the tackiness of silicone elastomers. *Surface and Interface Analysis*, *40*(3–4), 142–145.
- Nam, S., Vardar, Y., Gueorguiev, D., & Kuchenbecker, K. J. (2020). Physical variables underlying tactile stickiness during fingerpad detachment. *Frontiers in Neuroscience*, *14*, 235.
- Yeon, J., Kim, J., Ryu, J., Park, J. Y., Chung, S. C., & Kim, S. P. (2017). Human brain activity related to the tactile perception of stickiness. *Frontiers in Human Neuroscience*, *11*, 8.
- Moungou, A., Thonnard, J., & Mouraux, A. (2016). EEG frequency tagging to explore the cortical activity related to the tactile exploration of natural textures. *Scientific Reports*, *6*, 20738.
- Muñoz, F., Reales, J. M., Sebastián, M. A., & Ballesteros, S. (2014). An electrophysiological study of haptic roughness: Effects

- of levels of texture and stimulus uncertainty in the P300. *Brain Research*, 1562, 59–68.
30. Tang, W., Zhan, M. M., Chen, G. F., Liu, R., Peng, Y. X., Chen, S., Shi, Y. B., Hu, C. A., & Bai, S. J. (2021). Investigation of tactile perception evoked by ridged texture using ERP and non-linear methods. *Frontiers in Neuroscience*, 15, 676837.
 31. Chen, S., & Ge, S. R. (2017). Experimental research on the tactile perception from fingertip skin friction. *Wear*, 376, 305–314.
 32. Tang, W., Lu, X. Y., Chen, S., Ge, S. R., Jing, X. H., Wang, X. Y., Liu, R., & Zhu, H. (2020). Tactile perception of skin: Research on late positive component of event-related potentials evoked by friction. *Journal of the Textile Institute*, 111(5), 623–629.
 33. Jansen, B. H., & Rit, V. G. (1995). Electroencephalogram and visual evoked potential generation in a mathematical model of coupled cortical columns. *Biological Cybernetics*, 73(4), 357–366.
 34. Wendling, F., Bellanger, J. J., Bartolomei, F., & Chauvel, P. (2000). Relevance of nonlinear lumped-parameter models in the analysis of depth-EEG epileptic signals. *Biological Cybernetics*, 83(4), 367–378.
 35. Zhang, X. L., Lu, Y. J., Liu, E. Y., Yi, G. W., & Jia, J. H. (2012). Adhesion and friction studies of microsphere-patterned surfaces in contact with atomic force microscopy colloidal probe. *Colloids and Surfaces A: Physicochemical and Engineering Aspects*, 401, 90–96.
 36. Zhang, X. L., Wu, C. X., Mu, J. B., Bai, Y. M., Xie, H. L., & Jia, J. H. (2015). Adhesion and friction studies on silicon dioxide nanoparticle-textured surfaces prepared by the spin-coating process. *Journal of Adhesion Science and Technology*, 29(10), 1014–1025.
 37. Tang, W., Bhushan, B., & Ge, S. (2010). Friction, adhesion and durability and influence of humidity on adhesion and surface charging of skin and various skin creams using atomic force microscopy. *Journal of Microscopy*, 239(2), 99–116.
 38. Fogarty, J. S., Barry, R. J., & Steiner, G. Z. (2019). Sequential processing in the classic oddball task: ERP components, probability, and behavior. *Psychophysiology*, 56(3), e13300.
 39. Xie, Z., Jiao, J., Zhao, B., Zhang, J., & Xu, F. (2024). Theoretical and experimental research on the effect of bi-directional misalignment on the static and dynamic characteristics of a novel bearing. *Mechanical Systems and Signal Processing*, 208, 111041.
 40. Xie, Z., Li, J., Tian, Y., Du, P., Zhao, B., & Xu, F. (2024). Theoretical and experimental study on influences of surface texture on lubrication performance of a novel bearing. *Tribology International*, 193, 109351.
 41. Li, C. F., Zhang, T., Zang, X. L., Zhao, Z. Y., Fang, L. D., & Zhao, N. (2022). Void Fraction measurement based on flow noise decoupling and differential pressure. *IEEE Transactions on Instrumentation and Measurement*, 71, 9600312.
 42. Cai, J. H., & Chen, Q. Y. (2015). De-noising for NMR oil well logging signals based on empirical mode decomposition and independent component analysis. *Arabian Journal of Geosciences*, 9(1), 55.
 43. Suffczynski, P., Kalitzin, S., & Da Silva, F. H. L. (2004). Dynamics of non-convulsive epileptic phenomena modeled by a bistable neuronal network. *Neuroscience*, 126(2), 467–484.
 44. Schnepel, P., Kumar, A., Zohar, M., Aertsen, A., & Boucsein, C. (2015). Physiology and impact of horizontal connections in rat neocortex. *Cerebral Cortex*, 25(10), 3818–3835.
 45. Goryacheva, I., & Makhovskaya, Y. (2017). Combined effect of surface microgeometry and adhesion in normal and sliding contacts of elastic bodies. *Friction*, 5(3), 339–350.
 46. Polich, J. (2007). Updating P300: An integrative theory of P3a and P3b. *Clinical Neurophysiology*, 118(10), 2128–2148.
 47. Gray, H. M., Ambady, N., Lowenthal, W. T., & Deldin, P. (2004). P300 as an index of attention to self-relevant stimuli. *Journal of Experimental Social Psychology*, 40(2), 216–224.
 48. Donchin, E., & Isreal, J. B. (1980). Event-related potentials and psychological theory. *Progress in Brain Research*, 54, 697–715.

Publisher's Note Springer Nature remains neutral with regard to jurisdictional claims in published maps and institutional affiliations.

Springer Nature or its licensor (e.g. a society or other partner) holds exclusive rights to this article under a publishing agreement with the author(s) or other rightsholder(s); author self-archiving of the accepted manuscript version of this article is solely governed by the terms of such publishing agreement and applicable law.